Biomicrofluidics ARTICLE pubs.aip.org/aip/bmf

Optimization of upstream particle concentration from flow using AC electro-osmosis and dielectrophoresis

Cite as: Biomicrofluidics 18, 024105 (2024); doi: 10.1063/5.0189137
Submitted: 27 November 2023 · Accepted: 18 March 2024 ·
Published Online: 4 April 2024

Africa Smith de Diego,[1] Oreoluwa V. Griffiths,[2] Matthew P. Johnson,[2] Marco de Montis,[1,a)] and Michael Pycraft Hughes[2,3,a)]

AFFILIATIONS

[1]Kromek Ltd, Thomas Wright Way, Sedgefield, County Durham, TS21 3FD, United Kingdom
[2]Centre for Biomedical Engineering, University of Surrey, Guildford, Surrey GU2 7XH, United Kingdom
[3]Biomedical Engineering Department, Khalifa University, Sheikh Shakhbout bin Sultan St, Abu Dhabi, United Arab Emirates

[a)]**Authors to whom correspondence should be addressed:** marco.demontis@kromek.com and michael.hughes@ku.ac.ae

ABSTRACT

There are many applications where upstream sample processing is required to concentrate dispersed particles in flow; this may be to increase the concentration (e.g., to enhance biosensor accuracy) or to decrease it (e.g., by removing contaminants from flow). The AC electrokinetic phenomenon, dielectrophoresis (DEP), has been used widely for particle trapping for flow, but the magnitude of the force drops reduces rapidly with distance from electrode edges, so that nm-scale particles such as viruses and bacteria are only trapped when near the electrode surface. This limits the usable flow rate in the device and can render the final device unusable for practical applications. Conversely, another electrokinetic phenomenon, AC electro-osmosis (ACEO), can be used to move particles to electrode surfaces but is unable to trap them from flow, limiting their ability for sample cleanup or trap-and-purge concentration. In this paper, we describe the optimization of ACEO electrodes aligned parallel to pressure-driven flow as a precursor/preconditioner to capture particles from a flow stream and concentrate them adjacent to the channel wall to enhance DEP capture. This is shown to be effective at flow rates of up to 0.84 ml min^{-1}. Furthermore, the analysis of the 3D flow structure in the ACEO device by both simulation and confocal microscopy suggests that while the system offers significant benefits, the flow structure in the volume near the channel lid is such that while substantial trapping can occur, particles in this part of the chamber cannot be trapped, independent of the chamber height.

I. INTRODUCTION

There are a multitude of circumstances in lab-on-chip systems where particulates are present at low concentrations in a solute of interest. These solutes can be analytes (the target of a sensor system) or contaminants (particles present in a solution that is required to be contaminant-free). In either case, it is necessary to remove the particles from flow—either to concentrate them or to eliminate them.

In the former case, the detection of environmental pathogens such as viruses and bacteria is of significant interest for a range of purposes, including epidemiology, biosafety, and security. The field first came to prominence in the early 2000s, when attacks using posted, weaponized anthrax powder resulted in the death of five people and highlighted the need for rapid, *in situ* pathogen detection.[1] More recently, the global coronavirus pandemic in the early 2020s further highlighted the need for *in situ* pathogen detection in airports, hospitals, and public places.[2] In the alternative case, a solution might contain bacteria or nanoscale contaminants such as proteins, which might interfere with detection, requiring the removal of these contaminants from flow.

In the context of lab-on-chip systems, a common approach to particle manipulation is that of AC electrokinetics, a family of forces acting both on suspensoids and media that rely on the interactions of charge and divergent electric fields. Two are of particular

utility to particle concentration at surfaces. The first is dielectrophoresis (DEP), the induced force in dielectric particles suspended in non-uniform electric fields.[3] DEP can be attractive (positive DEP) or repulsive (negative DEP); with judicious electrode design, these have been used to concentrate particles in both continuous mode (where a constant inlet stream is divided in two, one of which contains all the particles) and batch modes (where particles are trapped from flow over a period of time and released all at once). The difficulty with using DEP for the trapping of nanoparticles is that the DEP force scales with particle volume and electric field gradient, so that a reduction in the particle volume requires a larger field gradient to facilitate capture. At the size of viruses, for example, the required gradients are such that trapping is only effective within a few μm of the electrode edges, which, in turn, limits throughput through the requirement for very narrow channel heights.[3]

A second phenomenon is AC electroosmosis (ACEO), where electric fields interact with the charges in the electrical double-layer directly above the electrode surface.[4] The tangential arc of the field can be considered as two orthogonal movement vectors—one acting toward the electrode surface and the other acting away from the inter-electrode edge. This second component creates a rapid flow of solution at the electrode surface, which then drives the movement of liquid at the surface in the direction away from the electrode edge.[5–9] Since the liquid must be replaced, fresh solution is drawn downward above the electrode edge. With a weaker electrohydrodynamic (EHD) force further inward from the electrode edge, the flow speed decreases, and a slow upward draft feeds back into the downdraft over the electrode edge to form a vortex. In 2003, it was shown that the effect could be used for particle concentration; instead of simply circulating particles in the vortices, the action of two adjacent vortices can trap particles in the stagnant area between them.[10,11]

The ACEO trapping effect has two primary advantages over DEP for particle trapping. First, it has been demonstrated to be capable of trapping particles over a wider range of particle sizes; when the speed of trapping was measured, it was found that ACEO trapping works at the same speed for particles ranging from proteins to large mammalian cells and including both bacteria and viruses.[12] Second, since the effect works on particles suspended within the flow "vortex" that is moved at the electrode edge and circulates across the cross section of the electrode chamber, anything within that circulation pattern will be trapped; experimental observations of the trapping of latex beads in a static chamber showed that all particles within 400 μm of the electrode surface could be trapped in the absence of flow.[13] In contrast, DEP forces are highly dependent on the proximity of the particles to the electrodes. Trapping particles more than 1–200 μm from the electrode surfaces requires high voltage, expensive equipment and limits the achievable flow speeds. These differences are summarized in Fig. 1.

ACEO has been studied under static flow conditions since the early 1990s[14,15] when an unusual particle collection regime occurred below 500 Hz, creating deposits on the center of electrode surfaces. The effects were observed again when Green and Morgan conducted experiments with narrow interdigitated electrodes. Below 500 kHz, particles with diameters of 93–216 nm accumulated along the axis of electrodes, while conventional DEP behavior resumed at higher frequencies.[9] From their observations, Green and Morgan concluded the deposit patterns were a result of DEP but with the additional finding that this was accompanied by an electrohydrodynamic force caused by electrolytes in the electrical double-layer across electrodes.[5] ACEO has primarily been applied for the concentration of bioparticles into static sensor surfaces[16,17,18] as a mechanism for driving fluid flow through asymmetric electrode design[18,19] or for mixing in microfluidic systems.[20]

Alternatively, electrodes can be aligned in parallel to the direction of flow in order to concentrate particles from flow onto a surface. Where the electrodes are parallel to the direction of pumped flow, the concentration effect serves to align particles within the flow. This was first demonstrated in 2014, when Hoettges *et al.*[21] used electrodes aligned principally along the direction of flow but with a slight angle (between 10° and 20°) to move particles to one side of the channel for concentration. A similar approach was adopted by Ren *et al.* in 2016,[22] using two electrodes with different widths to control particle collection via ACEO and, hence, concentrate to one outlet over the other. This was developed further by Han and Jang[23] who showed how ACEO electrodes arranged parallel to flow could be used to trap bacteria from pressure-driven flow, which were then

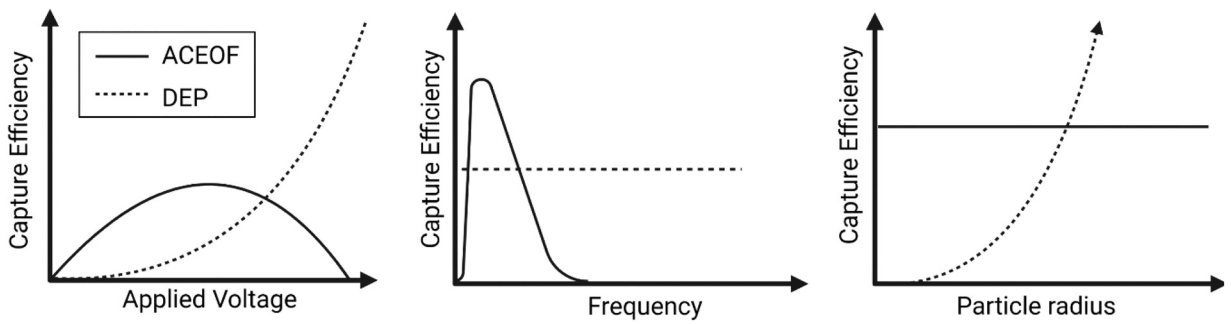

FIG. 1. Simplified trends of ACEO and pDEP capture for applied voltage, frequency, and particle radius. All plots assume constant F_{DEP} with Re[CM] > 0. Created with BioRender.

trapped using DEP on a biosensor. However, the flow rates used in that paper (between 50 and 1000 nl min^{-1}) were much lower than would normally be expected for detection applications, making the paper a proof of principle.

In this paper, we analyze the performance of combined ACEO–DEP microfluidic systems for particle capture at speeds approaching 1 ml.min^{-1}, using ACEO for upstream concentration particles from flow, streaming them into "beams" of particles adjacent to the electrode-bearing channel floor. We then use a separate DEP capture stage to further concentrate particles into batches. The ACEO stage is shown to be effective at flow rates of up to top limit of 0.84 ml min^{-1}, suggesting that higher throughputs may be achievable. However, the DEP stage efficiency drops at higher flow rates. Furthermore, we present the first combined use of confocal microscopy and finite element analysis (FEA) to understand the results, gaining new insights into the mechanisms occurring in ACEO trapping. These results suggest that while the system offers significant benefits, the flow structure in the volume of the channel nearest the lid is such that while substantial trapping can occur, particles in this part of the chamber cannot be trapped, independent of chamber height.

II. MATERIALS AND METHODS

A. Device construction

A custom-made device (Epigem Ltd., Redcar, UK) consisted of a PMMA cassette manufactured in two parts: one bearing a channel with 250 μm height and 2 mm width. Into this, two interdigitated electrode geometries were located. The first (aligned in the direction of flow) was for ACEO focusing and comprised electrodes arranged along the direction of flow. Electrodes were 10 mm long and 200 μm wide, with 100 μm inter-electrode spacing. The second array comprised electrodes for DEP trapping with 45 μm width and 45 μm gaps, aligned orthogonally to the direction of flow. The electrode arrangement is shown schematically in Fig. 2(a). The electrodes were fabricated using printed gold directly onto a PMMA substrate, onto which a PMMA lid with a machined channel 5 mm wide and 250 μm high was placed. Each device contained two parallel devices, and input and outputs were made using push-fit PMMA connectors. The assembled device is shown in Fig. 2(b). We also assessed the performance using a similar device but with different chamber heights of 150–500 μm to assess the effect of the chamber height on performance.

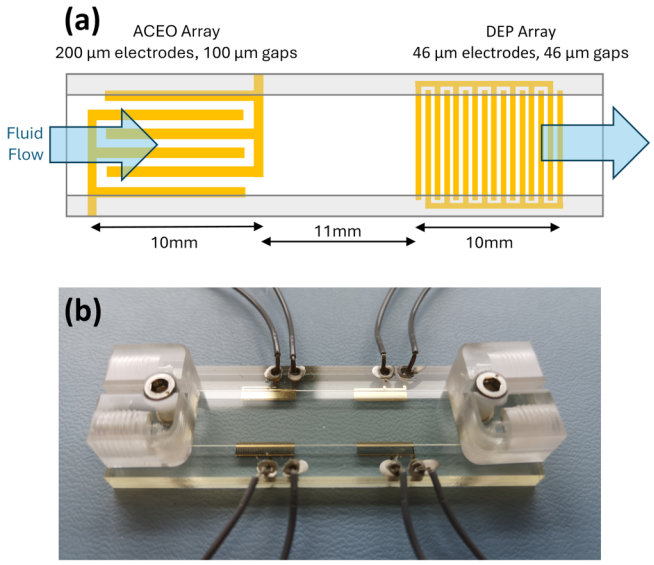

FIG. 2. (a) Schematic showing the electrode arrangement and dimensions and (b) photograph showing the manufactured cartridge.

B. Materials

Experiments were performed with three particle types: 1 μm polystyrene beads (Sigma-Aldrich, UK) and *Micrococcus luteus* (*M. luteus*) and *Escherichia coli* (*E. coli*) bacteria. Particles were suspended in aqueous solution at a concentration of 2.4%–2.6%, diluted to a concentration of 6×10^6 beads/ml in 0.25% pluronic acid solution, and then further diluted to 7.6×10^4 to enable accurate counting. To prepare the *M. Luteus* solutions, bacteria were cultivated overnight and the bacterial suspension was spun down at 2000g for 5 min, washed in 10 ml of 0.25% pluronic acid solution in water, pelleted again at 2000 g for 5 min, and resuspended in 1 ml of DI water containing 3 μl of Syto 9 Green dye. The bacterial cells were incubated with the dye for 30 min protected from light and then spun down at 2500 g for 5 min. The pellet was resuspended in 1 ml of DEP buffer, spun down at 2500 g for 5 min, and resuspended again in 1 ml of DEP buffer to reduce the background fluorescence of the solution. This stock solution of dyed bacteria was diluted down using 0.25% pluronic acid solution until an OD600 of 0.01 was obtained, which was subsequently used for the ACEO. To prepare *E.coli* solutions, bacteria were cultured in aqueous nutrient broth. 5 ml of nutrient broth containing 140×10^6 cells/ml was centrifuged at 3000 g for 4 min, and the pellet was resuspended in 10 ml 0.25% pluronic acid and pelleted again under the same conditions before the pellet was resuspended again in 10 ml 0.25% pluronic acid. A cell count of this bacterial suspension was taken and dilution adjusted to 20×10^6 cells/ml for analysis.

C. Performance assessment

Using 50 ml syringes, the 7.6×10^4 1 μm bead solution was fed into the cartridge, with a Razel A-99 syringe pump. The speed of infusion ranged from 8.4 to 840 μl/min. A signal generator was connected to the ACEO electrodes to produce signals between 0 and 20 V_{p-p} and from 150 to 200 Hz. To evaluate the efficiency of ACEO flow to concentrate particles from the bulk fluid at the electrode surface, the solution was run for 1 min to allow the flow to reach steady state, and then beads were counted at the electrode surface, which was compared to the number of beads estimated in the volume above the electrodes assuming homogeneous dispersion. Above 59 μl/min, it was not possible to accurately count the beads due to image blurring.

We also used *M. luteus* to assess the effect of the flow rate and chamber height on overall trapping. For these experiments, a solution of dyed *M. luteus* was flowed through the device and four 50 μl fractions were collected. These initial fractions were used to determine the baseline fluorescence when the electrodes were not energized. Then, the DEP electrodes were energized by applying a constant signal (180 Hz, 20 V_{pp}), and the mean fluorescence of the fractions collected was compared to the initial baseline fluorescence. The percentage capture was calculated using the following formula:

$$\text{Capture efficiency} = \frac{\text{mean baseline fluorescence} - \text{mean DEP capture fluorescence}}{\text{mean baseline fluorescence}}.$$

This method was used to determine the influence of either the flow rate (from 25 to 100 μl/min) or chamber height (from 150 to 500 μm) on the capture efficiency.

D. ACEO/DEP trapping experiments

The experimental cartridges were designed with two sets of electrodes: the ACEO and DEP trapping electrodes. The DEP electrodes were energized at higher frequencies from 10 kHz to 1 MHz and voltages from 10 to 20 V_{p-p}. For these experiments, after the aliquots were collected, spectrophotometric analysis was used to quantify the changes in 1 μm bead concentration. The stock concentration of 6×10^6 was used without dilution. For each signal and speed condition, an aliquot was taken in the absence of any electric fields and then the ACEO signal was switched on and allowed to develop for one minute. The DEP electrodes were then energized, and the aliquot of interest was taken after 1 min with both electrode arrays energized. Spectrophotometric absorbance values for the two aliquots were compared for each condition to calculate trapping efficiency.

To assess whether bacterial cells were influenced to a similar degree as 1 μm beads in the experimental cartridges, the ACEO/DEP trapping experiments were repeated with the *E. coli* suspension, aliquoting both before and after signal application. To provide comparable data and based upon previously successful conditions, a frequency of 1 MHz and a voltage of 20 V were used at the DEP electrodes. The aliquots were analyzed through the manual counting of *E. coli* cells via a hemocytometer and the change in the concentration before and after signal application defined the trapping efficiency.

E. Confocal microscopy

A Nikon AM1 confocal microscope was used to image the action of ACEO in the experimental cartridges. The chips were imaged on the confocal microscope, chips were infused with 1 μm polystyrene beads at 6×10^6 beads/ml in 0.25% pluronic acid, and the chip was stoppered to create a static environment. After the ACEO electrodes were energized using the signal generator, their position in the xyz planes was located. The ACEO action was allowed to settle for 2 min. before a "Z-stack" image was taken, whereby an image was taken in the Z-plane from the bottom of the electrodes to the top of the chip's internal chamber. An image was taken at 0.5 μm increments, these images were then stacked together to produce a 3D image of the internal chamber of the cassettes.

F. Simulation

A finite element model of ACEO trapping in flow was developed on Comsol Multiphysics to better understand the influence of the electrode width and inter-electrode spacing on the ACEO vortexes generated. Simulations were performed using the Electroosmotic Flow component in the standard Microfluidics module for Comsol, using a swept mesh, and solved the frequency domain for the electroosmotic flow, a stationary study for the laminar flow and a time dependent study for particle tracking. The electric currents module was used to model the electric field. The driven electrode was powered with 20 V, while the grounded electrode had the condition V = 0. The laminar flow module was used with the boundary condition relating to the electric double-layer defining the electroosmotic flow. The frequency of the signal modeled was 180 Hz, in line with experiments. One study containing a stationary step was used to solve the initial conditions and to generate the ACEO flow. A secondary stationary step was used to generate the initial stationary values of the electric field. A final time dependent study was used to generate the values of the ACEO flow at a range from 0 to 0.05 s in 0.01 s time steps. The fluid flow velocity and streamlines were generated in the middle of the electrodes under the different conditions tested.

III. RESULTS AND DISCUSSION

A. ACEO focusing

We first investigated the use of interdigitated electrodes aligned along the direction of flow to concentrate the particles present in the center of the chamber and focus them toward the chamber floor, using multiple combinations of flow rates and electrode potential. Images of flow at two different flow rates and six different energizing voltages can be seen in Fig. 3(a) (see also multimedia view). In all cases, ACEO-driven trapping was observed. At lower voltages, the vortices were relatively weak, resulting in less collection, with more particles remaining in the vortices, while the vortices from the two electrode edges were not sufficiently large to meet. This resulted in two separate collections on top of the electrodes, one from each vortex. At higher voltages, the two collection "fronts" were moved closer together, finally merging above 14 V_{pp}. At the highest potentials, the width of the single focused particle "beam" was observed to narrow.

To determine the efficacy of trapping, we analyzed the number of particles on the electrode and compared this to the number expected in the volume directly above. This necessitated the use of larger (1 μm diameter) beads and lower concentrations and flow rates to observe the particles effectively. In these experiments [shown graphically in Fig. 3(b)], we found that the capture efficiency increased with applied voltage for the lowest speed (8.4 ul/min), in line with expectations; the trend was less apparent

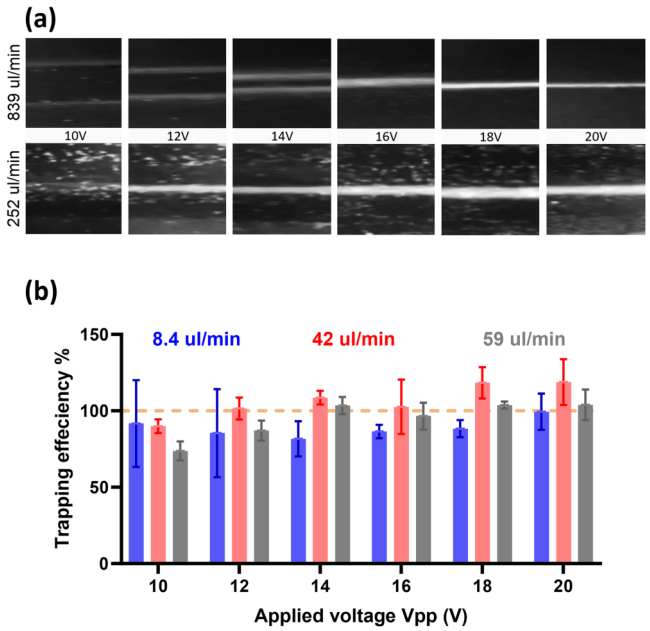

FIG. 3. Differences in the ACEO trapping behavior at two flow rates and six different applied potentials. (b) The percentage of particles trapped in the flow for different flow rates and applied voltages. Multimedia available online.

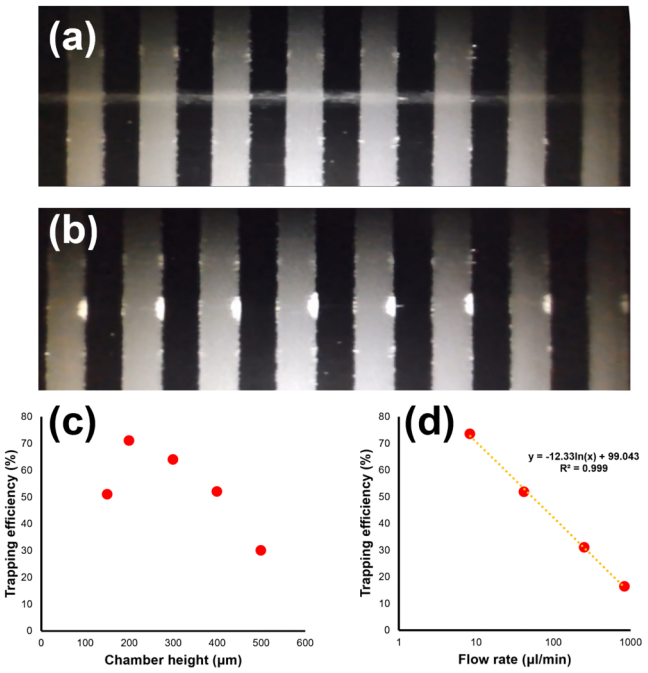

FIG. 4. The DEP section of the array (a) before and (b) after the application of voltage to the array. See also integrated video (multimedia view). Electrodes are gray vertical bands, and inter-electrode gaps are black. (c) and (d) The trapping efficiency of the DEP array as a function of chamber height (c) and flow rate (d); the former exhibited an optimum around 2–300 μm, while the latter showed a logarithmic decline over the flow rate range. Multimedia available online.

for higher voltages at the higher two flow speeds. While the flow rates increased from 8.4 to 59 ul/min (an increase of 7×), the capture efficiencies showed similar trapping potential, particularly above 16 V_{pp}, a result in contrast to DEP, which was highly affected by flow rate. As can be seen in Fig. 3, capture efficiency was occasionally greater than 100%; this was also observed in "zipper" electrodes, where some collection sites were occasionally observed to partially empty into adjacent electrodes, increasing the number of trapped particles beyond that expected where they were distributed homogeneously.[12]

When we observed the flow of particles at different heights above the electrode layer, we found that while particles were trapped in vortices nearer the electrodes, nearer the chamber roof they appeared to pass over the electrodes unimpeded. The larger particles ultimately descended from this layer by sedimentation and were trapped in vortices, in line with observations by Mohtar *et al.*[13]

B. ACEO/DEP trapping efficiency

Following the ACEO stage, we observed DEP trapping in the second electrode array using *M. luteus* spores. At low flow speeds, particle trapping was high due to the location of the particles in flow immediately above the electrode surface, which acted on the particle stream from the ACEO section. An example of this can be seen in Figs. 4(a) and 4(b) (multimedia view). As with the ACEO section, we were able to quantify trapping efficiency; since the trapped particles were stationary (unlike those in the focused beams in ACEO), it was possible to determine overall efficacy across a range of conditions, as shown in Figs. 4(c) and 4(d). As can be seen in Fig. 4(c), the alteration of the chamber height yielded an optimum of around 200–300 μm, with performance reducing rapidly for variations from this; notably, data from 200 μm and upwards suggest a curve that is asymptotic toward 80%, in line with simulations, with only the 150 μm value deviating from this and potentially indicating other factors becoming important at low chamber heights. Figure 4(d) shows that trapping was strongly adversely affected by higher flow rates, where the drag force due to fluid flow was too large to be overcome by DEP, reducing the trapping efficiency.

C. Simulation and confocal microscopy

The movement of suspensoids interacting with DEP field gradients is well-characterized,[3] but the flow through ACEO trapping is more complex and less well studied. A previous study by Melvin *et al.* simulated ACEO vortex formation within a static volume[18] but did not look into driven flows. In order to address this and to better understand the motion of particles in the ACEO section under a driven flow, we employed FEA simulation to study vortex formation within our chips. To ensure the accuracy of the model, we employed the confocal microscopy of particle positions inside

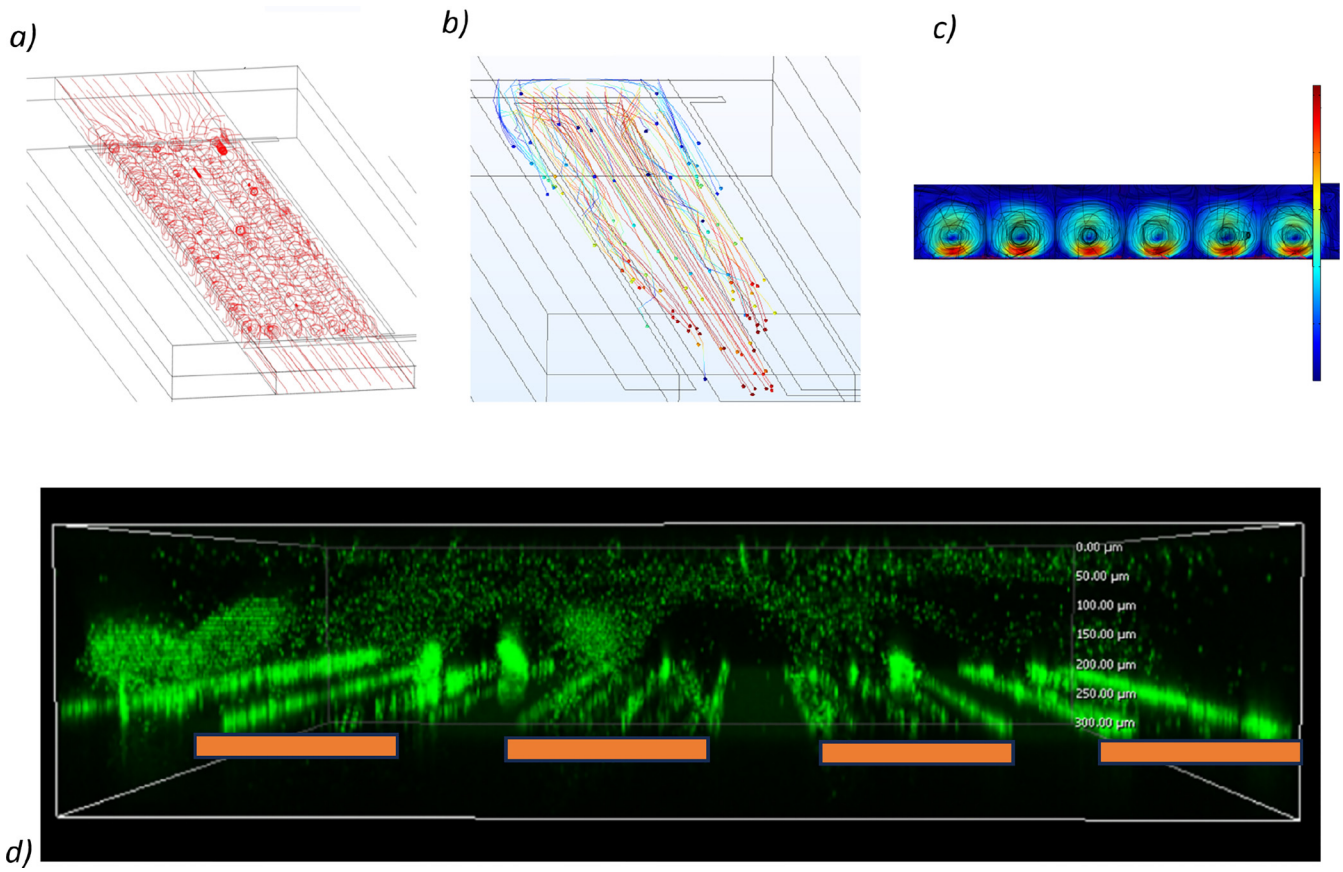

FIG. 5 (a)–(c) Simulations of the fluid flow in the ACEO section of the chip, showing (a) the vortices at the chip edge, (b) particle trajectories concentrating particles toward the electrode surface, directly above the electrode center, and (c) the velocity and direction of a 2D slice through the electrodes. (d) A 3D confocal microscopic image of fluorescent beads in the ACEO electrode, showing areas of concentration on the electrodes, and depletion in the vortices. The orange rectangles indicate the location of the electrodes.

the device to observe particle motion and validate observations in the model.

The simulation of fluid flow in electrodes undergoing an ACEO regime used a full 3D model of the electrodes and interelectrode spaces in our physical 3D electrode array; a representative image showing the model can be seen in Figs. 5(a) and 5(b). We examined the cross sections through the chamber to understand the relationship between the vortices and the enclosing chamber, as shown in Fig. 5(c). The simulation showed vortex formation creates approximately circular regions, which would be depleted of particles, but that these vortices only extended to approximately 80% of the channel height, with the counter-rotating upper eddies formed between the ACEO vortices and the chamber roof, consistent with classical lid-driven cavity problems.[24] To validate this simulation, we used confocal microscopy to observe the motion of beads undergoing ACEO flow in our device. The nature of confocal microscopy means that a single snapshot image cannot be taken, but with sufficient beads flowing under steady-state conditions, it is possible to observe the locations of particle collection and depletion. A typical image of the observed inter-electrode space can be seen in Fig. 5(d), which shows a number of key features associated with both conventional 2D microscopy and with the simulations described above.

As expected, the highest particle concentrations are observed in the "beams" above the electrode surface, which are notably taller than wide when observed from this perspective. Large, quasi-circular dark regions define the location of the vortices, which have been cleared of the beads that have collected on the electrode surfaces. Finally, it is possible to identify the boundary suggested by simulation; at the top of the chamber, it is possible to identify smaller circular dark regions, suggesting the presence of counter-vortex behavior. Again, the maximum reach of the vortices appears to be approximately 80% of the chamber height, suggesting a hard limit due to the limits of lid-driven cavity flow.[24]

With the model having been validated by confocal microscopy, we investigated whether the upper eddy counter-vortices

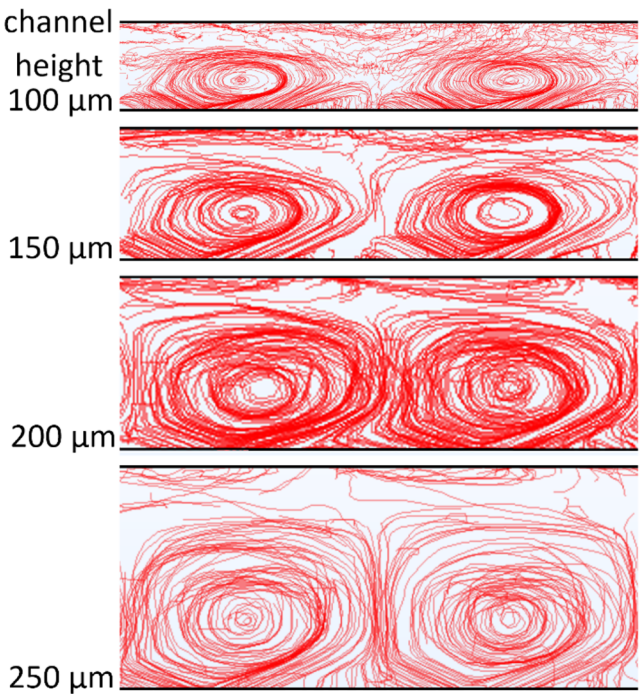

FIG. 6. Comsol simulations of fluid motion in a cross section above the electrodes, showing the vortices on either side of an inter-electrode gap, at four different chamber heights. A smaller dead space, containing either no movement or counter-vortices, can be visible in the upper portion of each chamber height.

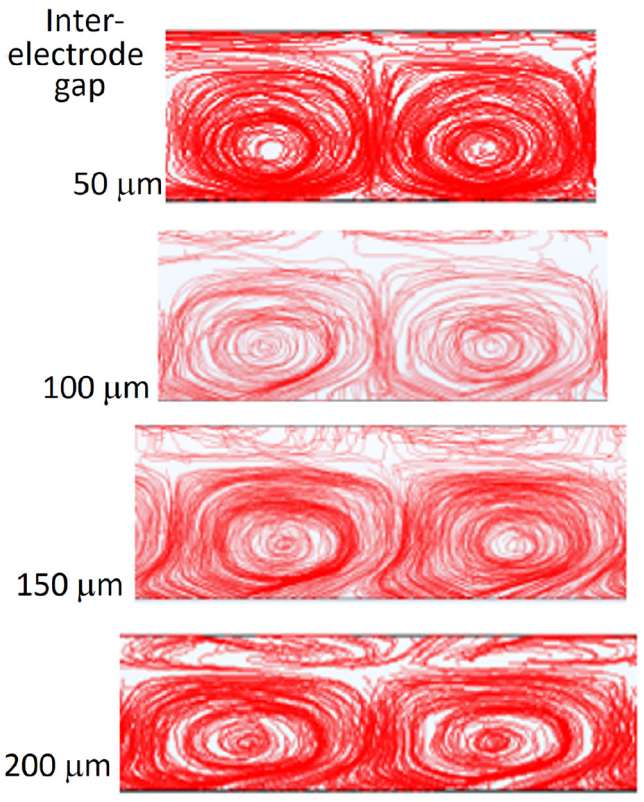

FIG. 7. Comsol simulations of fluid motion in a cross section above the electrodes, showing the vortices on either side of an inter-electrode gap, for four different gap widths.

could be lessened by the reduction in the chamber height close to the unrestricted reach of the ACEO vortices. To address this, we simulated fluid flow using three lower chamber heights to see whether a threshold could be reached where the vortices encompassed the whole volume. Instead, the simulations (visible in Fig. 6) showed that the effect scaled with chamber height; even when the chamber height was reduced by 60%, a region of counterflow and dead space was identified in the top portion of the chamber. Similarly, the height of the divisor between the primary vortex and countervortex appears independent of the width of the inter-electrode gap, according to simulations (Fig. 7). This would mean that any ACEO-driven particle collector may ultimately be limited to a maximum 70%–80% efficiency due to the presence of these counter-vortices, unless the chamber roof could be engineered to better manage vortex flow. This might be achieved by machining grooves following the ACEO vortices along the length of the chamber ceiling or by artificially increasing the surface roughness with a textured coating to increase turbulence with the intention of mixing the particles within the upper eddies into the larger ACEO vortices below. Considering the results in Figs. 4(c) and 4(d) in light of the simulations in Fig. 6 suggests that at low chamber height, the primary factor limiting trapping is the high flow rate caused by the restriction of the cross-sectional area of the channel, whereas for higher sizes, the limitation is more likely due to the increased size of the counter-eddy dead zones above the vortices.

IV. CONCLUSIONS

We have investigated the application of combined two-stage ACEO–DEP devices for enhanced trapping of particles for upstream concentration and depletion applications. The system used interdigitated ACEO electrodes aligned parallel to the field, followed by DEP electrodes aligned orthogonally to the flow. Testing using microbeads suggests that ACEO concentration from flow is largely independent of flow speed up to 1 ml min^{-1} and potentially higher but that DEP trapping is more limited and may need optimization in order to be able to trap sufficient particles at higher flow rates, for example, by employing a different chamber height at the DEP stage to reduce the flow rate for trapping or by reducing inter-electrode gaps. Moreover, by analyzing particle concentration using confocal microscopy and comparing the result to simulations of fluid flow, we have further explored the "dead zones" above the trapping vortices caused by cavity-driven upper eddies, which cannot be eliminated by chamber height scaling.

ACKNOWLEDGMENTS

This work was funded by Kromek Ltd. M.P.J. received a partial PhD scholarship from Deparator Ltd. M.P.H. received partial funding from Khalifa University (No. FSU-2022-20).

AUTHOR DECLARATIONS

Conflict of Interest

The authors have no conflicts to disclose.

Author Contributions

A.S.d.D. and O.V.G. contributed equally to this work.

Africa Smith de Diego: Formal analysis (equal); Software (equal); Visualization (equal); Writing – original draft (supporting); Writing – review & editing (supporting). **Oreoluwa V. Griffiths:** Investigation (equal); Methodology (equal); Visualization (lead); Writing – original draft (supporting); Writing – review & editing (supporting). **Matthew P. Johnson:** Conceptualization (equal); Investigation (equal); Methodology (equal). **Marco de Montis:** Conceptualization (equal); Funding acquisition (equal); Investigation (equal); Project administration (equal); Supervision (equal); Writing – original draft (supporting); Writing – review & editing (supporting). **Michael Pycraft Hughes:** Conceptualization (lead); Formal analysis (supporting); Funding acquisition (equal); Methodology (equal); Project administration (equal); Supervision (lead); Writing – original draft (lead); Writing – review & editing (lead).

DATA AVAILABILITY

The data that support the findings of this study are available from the corresponding authors upon reasonable request.

REFERENCES

[1]National Research Council, *Review of the Scientific Approaches Used During the FBI's Investigation of the 2001 Anthrax Letters* (National Academies Press, 2011).
[2]B. Singh, B. Datta, A. Ashish, and G. Dutta, "A comprehensive review on current COVID-19 detection methods: From lab care to point of care diagnosis," Sens. Int. **2**, 100119 (2021).
[3]R. Pethig, *Dielectrophoresis Theory, Methodology and Biological Applications* (John Wiley & Sons Inc., Hoboken, 2017).
[4]M. Z. Bazant, M. S. Kilic, B. D. Storey, and A. Ajdari, "Towards an understanding of induced-charge electrokinetics at large applied voltages in concentrated solutions," Adv. Colloid Interface Sci. **152**, 48–88 (2011).
[5]N. Green, A. Ramos, A. Gonzalez, H. Morgan, and A. Castellanos, "Fluid flow induced by nonuniform ac electric fields in electrolytes on microelectrodes. I. Experimental measurements," Phys. Rev. E **61**, 4011–4018 (2000).
[6]A. Ramos, P. Garcia-Sanchez, and H. Morgan, "AC electrokinetics of conducting microparticles: A review," Curr. Opin. Colloid Interface Sci. **24**, 79–90 (2016).
[7]A. Gonzalez, A. Ramos, N. Green, A. Castellanos, and H. Morgan, "Fluid flow induced by nonuniform ac electric fields in electrolytes on microelectrodes. II. A linear double-layer analysis," Phys. Rev. E **61**, 4019–4028 (2000).
[8]N. G. Green, A. Ramos, A. Gonzalez, H. Morgan, and A. Castellanos, "Fluid flow induced by nonuniform ac electric fields in electrolytes on microelectrodes. III. Observation of streamlines and numerical simulation," Phys. Rev. E **66**, 026305 (2002).
[9]N. G. Green and H. Morgan, "Separation of submicrometre particles using a combination of dielectrophoretic and electrohydrodynamic forces," J. Phys. D: Appl. Phys. **31**, L25–30 (1998).
[10]K. F. Hoettges, M. B. McDonell, and M. P. Hughes, "Use of combined dielectrophoretic/electrohydrodynamic forces for biosensor enhancement," J. Phys. D: Appl. Phys. **36**, L101–L104 (2003).
[11]K. F. Hoettges, M. P. Hughes, A. Cotton, N. A. Hopkins, and M. B. McDonnell, "Optimizing particle collection for enhanced surface-based biosensors," IEEE Eng. Med. Biol. **22**, 68–74 (2003).
[12]Y. Hubner, K. F. Hoettges, M. B. McDonnell, M. J. Carter, and M. P. Hughes, "Applications of dielectrophoretic/electrohydrodynamic 'zipper' electrodes for detection of biological nanoparticles," Int. J. Nanomed. **2**, 427–431 (2007).
[13]M. N. Mohtar, K. F. Hoettges, and M. P. Hughes, "Factors affecting particle collection by electro-osmosis in microfluidic systems," Electrophoresis **35**, 345–351 (2014).
[14]R. Pethig, Y. Huang, X.-B. Wang, and J. P. H. Burt, "Positive and negative dielectrophoretic collection of colloidal particles using interdigitated castellated microelectrodes," J Phys. D: Appl. Phys. **25**, 881 (1992).
[15]J. A. Price, J. P. Burt, and R. Pethig, "Applications of a new optical technique for measuring the dielectrophoretic behaviour of micro-organisms," Biochim. Biophys. Acta **964**, 221–230 (1988).
[16]H. O. Fatoyinbo, K. F. Hoettges, S. M. Reddy, and M. P. Hughes, "An integrated dielectrophoretic quartz crystal microbalance (DEP-QCM) device for rapid biosensing applications," Biosens. Bioelectron. **23**, 225–232 (2007).
[17]N. A. P. Ondevilla, T.-W. Wong, N.-Y. Lee, and H.-C. Chang, "An AC electrokinetics-based electrochemical aptasensor for the rapid detection of microRNA-155," Biosens. Bioelectron. **199**, 113847 (2022).
[18]E. M. Melvin, B. R. Moore, K. H. Gilchrist, S. Grego, and O. D. Velev, "On-chip collection of particles and cells by AC electroosmotic pumping and dielectrophoresis using asymmetric microelectrodes," Biomicrofluidics **5**, 034113 (2011).
[19]C. C. Chung, T. Glawdel, C. L. Ren, and H. C. Chang, "Combination of ac electroosmosis and dielectrophoresis for particle manipulation on electrically-induced microscale wave structures," J. Micromech. Microeng. **25**, 035003 (2015).
[20]W. Y. Ng, S. Goh, S. Y. C. Lam, C. Yang, and I. Rodríguez, "DC-biased AC-electroosmotic and AC-electrothermal flow mixing in microchannels," Lab Chip **9**, 802–809 (2009).
[21]K. F. Hoettges, M. B. McDonnell, and M. P. Hughes, "Continuous flow nanoparticle concentration using alternating current-electroosmotic flow," Electrophoresis **35**, 467–473 (2014).
[22]Y. Ren, J. Liu, W. Liu, Q. Lang, Y. Tao, Q. Hu, L. Hou, and H. Jiang, "Scaled particle focusing in a microfluidic device with asymmetric electrodes utilizing induced charge electroosmosis," Lab Chip **16**, 2803 (2016).
[23]C.-H. Han and J. Jang, "Integrated microfluidic platform with electrohydrodynamic focusing and a carbon nanotube-based field-effect transistor immunosensor for continuous, selective, and label-free quantification of bacteria," Lab Chip **21**, 184 (2021).
[24]P. N. Shankar and M. D. Deshpande, "Fluid mechanics in the driven cavity," Annu. Rev. Fluid Mech. **32**, 93–136 (2000).